JOURNAL OF Materials CHEMISTRY

Cation partitioning in ternary vanadium sulfides AV_2S_4 (A = Ti, Cr, Fe, Ni)

Anthony V. Powell,* Douglas C. Colgan and Paz Vaqueiro

Department of Chemistry, Heriot-Watt University, Riccarton, Edinburgh, UK EH14 4AS

Received 17th August 1998, Accepted 22nd October 1998

A combination of time-of-flight powder neutron diffraction and powder X-ray diffraction has been used to investigate changes in the cation distribution in a series of isostructural (space group $I2/m$ $a \approx 5.9$, $b \approx 3.3$ $c \approx 11.3$Å, $\beta \approx 92°$) ternary vanadium sulfides, AV_2S_4 (A = Ti, Cr, Fe, Ni). A progressive change from an inverse Cr_3S_4 structure, when A is drawn from the left of the transition series, to a normal Cr_3S_4 structure, when A is drawn from the right of the series, occurs. The magnetic susceptibility of all materials has a significant temperature-independent component and both spin-glass behaviour [A = Cr, $T_g = 15(3)$ K] and long-range magnetic order [A = Fe, $T_N = 135(3)$ K] are observed.

Introduction

Much of our recent research has been concerned with the structural and physical properties of ternary sulfides with the Cr_3S_4 structure.[1–4] This is an ordered vacancy structure[5] (Fig. 1) which can be considered to be intermediate between that of NiAs, in which cations occupy octahedral sites between all pairs of hexagonally close-packed anion layers, and that of CdI_2, in which sites between alternate pairs of anion layers are vacant. In the Cr_3S_4 structure, sites between pairs of anion layers are alternately fully and half occupied giving rise to a stacking sequence which may be represented schematically as $\cdots XMXM_{0.5}XMX\cdots$ Cations in the half-occupied layer occupy the available sites in an ordered manner, resulting in a two-dimensional, $\sqrt{3}a_p \times a_p$, superstructure. The Cr_3S_4 structure is the prototype for the structures of a variety of ternary sulfides of general formula AM_2S_4 for which it provides an alternative to the spinel structure.[6] For ternary materials, two extreme structures, differing in the distribution of cations between the two crystallographically distinct sites, can be envisaged. These correspond to the normal, $(A)[M_2]S_4$, and inverse, $(M)[AM]S_4$ structure types, where parentheses and square brackets represent sites in the vacancy and fully occupied layers respectively.

Although relatively few detailed structural studies[2,3,7–9] have been performed on ternary Cr_3S_4-type chalcogenides, the available data suggest that site-preference effects in materials containing cations from adjacent groups of the periodic table are small. By contrast, transition series cations drawn from groups of the periodic table which are more widely separated exhibit more marked site preferences. Consequently there is a greater tendency for cation partitioning in such materials. For non-stoichiometric materials, the cation distribution may be sensitive to composition and related to changes in the physical properties. For example, in the series $V_xCr_{3-x}S_4$ $(0 \leqslant x \leqslant 1)$, the change from metallic to semiconducting behaviour which occurs with increasing vanadium content, and is accompanied by the loss of long-range magnetic order,[1] appears to be associated with an abrupt change from a normal structure type to an intermediate structure at a critical composition $x_c \approx 0.4$.[2] The analogous nickel-containing series shows considerably less structural variation: the adoption of a near normal structure at all compositions is reflected in physical properties which show remarkably little compositional dependence.[3]

A systematic study of the site-preferences of transition-metal cations in the Cr_3S_4 structure requires series of isostructural compounds in which either the A or M cation may be varied independently within a metal sulfide matrix. However, as the spinel structure is preferred over the Cr_3S_4-type for certain combinations of cations, the range of many such series is restricted. The compounds AV_2S_4 provide one of the more complete series as, in addition to the binary sulfide V_3S_4, Cr_3S_4-type structures are adopted for A = Ti, Cr, Mn, Fe, Ni. The members of this series therefore provide an opportunity to investigate the change in site-preference of divalent transition-metal cations across the transition series whilst maintaining an effectively constant vanadium sulfide framework.

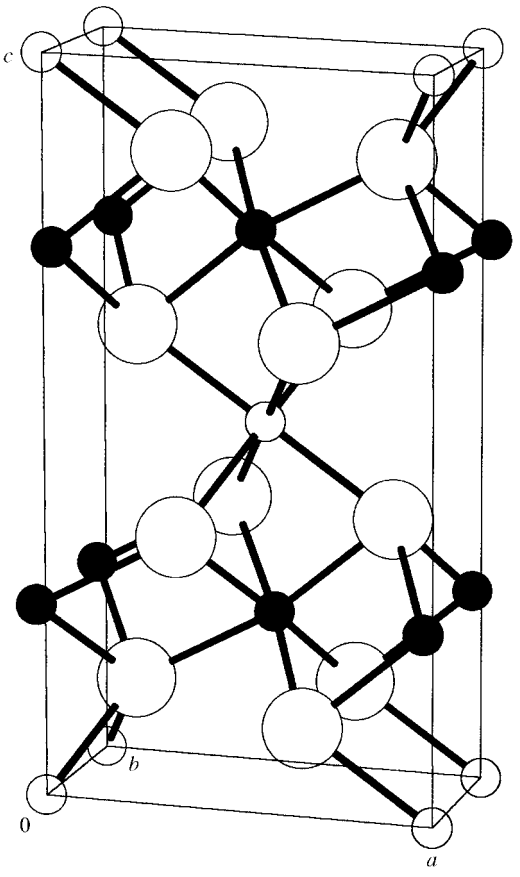

Fig. 1 The ordered defect structure of Cr_3S_4. Large open circles represent anions, small filled circles represent cations in the fully occupied layer and small open circles represent cations in the vacancy layer.

The material of nominal composition MnV_2S_4 has been shown[10] to be a mixture of MnS and a Cr_3S_4-type phase of uncertain stoichiometry. It was therefore excluded from the present study which reports the structural behaviour of phases of general formula AV_2S_4 (A = Ti, Cr, Fe, Ni). The combination of the low contrast between the cations involved, which is afforded by X-rays, and the vanishingly small neutron scattering length of vanadium necessitated simultaneous use of data from both techniques in Rietveld refinement.

Experimental

All samples were prepared by a conventional high-temperature technique. Appropriate mixtures of high-purity metal powders and sulfur were ground in an agate pestle and mortar prior to sealing into evacuated (10^{-4} Torr) silica ampoules. All mixtures were prepared with a slight deficiency of sulfur, as in previous work.[1] Mixtures were fired at elevated temperatures for periods of up to 10 days, with intermittent regrinding. The titanium-containing sample was initially fired at a lower temperature of 823 K in order to minimise reaction with the quartz ampoule which had previously been observed with the early transition series metals at high temperatures. Reaction progress was monitored by collecting powder X-ray diffraction patterns between each firing and reactions were deemed to be complete when successive firings produced no further changes in diffraction patterns. Reaction times and final firing temperatures are shown in Table 1. Metal contents were determined by analytical electron microscopy using a Hitachi S-2700 scanning electron microscope fitted with a PGT IMIX-XE detection system. This enabled quantitative analysis to be performed without the use of intensity standards. Sulfur contents were determined by oxidising the samples in a flow of dry air on a Stanton Redcroft STA-780 thermobalance. Powder X-ray diffraction patterns were collected on a Philips PA2000 powder diffractometer, with nickel-filtered Cu-Kα radiation, in step-scan mode over the angular range $5 \leqslant 2\theta/^\circ \leqslant 100$ in steps of $2\theta = 0.02^\circ$ and counting times of 5 s per step. The high crystallinity of the products necessitated wet-grinding of samples with ethanol prior to data collection. Magnetic susceptibility measurements on powdered samples were made using a Quantum Design MPMS2 SQUID susceptometer. Samples were contained in gelatin capsules and data collected over the temperature range $5 \leqslant T/\mathrm{K} \leqslant 300$ both after cooling the sample in zero applied field (zfc) and after cooling in the measuring field (fc) of 1000 G. Data were corrected for the diamagnetism of the capsule and for intrinsic core diamagnetism. The electrical resistance of the samples was measured by the four-probe DC technique. An ingot ($\approx 6 \times 3 \times 1$ mm) was cut from a sintered pellet, four 50 μm silver wires were attached using colloidal silver paint and connections made to a HP34401A multimeter. Measurements over the temperature range $80 \leqslant T/\mathrm{K} \leqslant 300$ ($80 \leqslant T/\mathrm{K} \leqslant 350$ in the case of CrV_2S_4) were made by placing the sample in an Oxford Instruments CF1200 cryostat connected to an ITC502 temperature controller.

Time-of-flight powder neutron diffraction data were collected on the Polaris diffractometer at the ISIS spallation source, Rutherford Appleton Laboratory, Oxon. In each case data were collected on *ca.* 3 g of sample contained in thin-walled vanadium cans. Initial data manipulation and reduction was carried out using Genie[11] spectrum manipulation software. Rietveld refinement was performed with the GSAS[12] suite of programs installed on the Heriot-Watt University Alpha 2100–4275 system.

Results

Initial structural characterisation indicated all materials to be single phases, isostructural with Cr_3S_4, whose unit-cell parameters are similar to those previously reported.[13–15] However, trace amounts of oxide impurities were identified in the samples by analytical electron microscopy. In all cases other than that of CrV_2S_4, such impurities are at an extremely low level and the uncertainties introduced into the analytically determined compositions of Table 1 are therefore slight. A slightly greater level ($\leqslant 1.3\%$ by weight) of oxide impurity in CrV_2S_4 introduces an error into the thermogravimetric data which is likely to be the cause of the discrepancy between analytically and crystallographically determined compositions.

Neutron data from the highest resolution back-scattering bank of detectors in the time-of-flight range 6000–19300 μs ($d \approx 1.0$–3.5 Å) were summed and normalised. X-ray data in the angular range $20 \leqslant 2\theta/^\circ \leqslant 100$ ($d \approx 1.0$–4.4 Å) were used. In order to facilitate comparison between data from the two techniques, units of *d*-spacing are used throughout this work. Refinements were initiated in the space group *I*2/*m* using atomic coordinates previously determined[2] for VCr_2S_4 for the initial structural model. Neutron scattering lengths and X-ray scattering factors incorporated within the GSAS program were used. The backgrounds of both the X-ray and the neutron profiles were modelled using a cosine Fourier series with the coefficients included as refinable parameters. The X-ray peak shape was described by a pseudo-Voigt function whereas that for the neutron profile was a convolution of a Gaussian with a double exponential function.

The initial structural model for the ternary phases involved occupation of sites in the fully occupied layer by vanadium only, whilst the vacancy layer sites were exclusively occupied by the A-cation. A weak feature evident at a *d*-spacing of 2.140 Å in the neutron data for CrV_2S_4, and obscured by overlapping reflections from the ternary sulfide in the other profiles, has previously been identified[2] as the (110) reflection of vanadium ($d_{\mathrm{calc}} = 2.141$ Å) of instrumental origin. In addition, a broad and diffuse feature centred at *ca.* 2.2 Å was common to all profiles. This may be assigned as the (113) reflection of V_2O_3 ($d_{\mathrm{calc}} = 2.186$ Å) which has previously been shown to be a contaminant in ternary vanadium sulfides.[16,17] Only in the case of CrV_2S_4 was this feature of sufficient intensity to permit a two-phase Rietveld refinement to be performed. Using available structural data[18] for V_2O_3, an estimate of 1.3% by weight of V_2O_3 in this sample was obtained: the level in the remaining samples is significantly lower. Owing to the very low levels of oxide impurity, the region 2.13–2.20 Å was excluded from the structural refinement of all phases. Additional weak features were evident in

Table 1 Results of thermogravimetric analysis and energy dispersive X-ray microanalysis for AV_2S_4 phases

Nominal composition	Final firing temperature/K	Total firing time/days	Nominal A:V	Experimentally determined A:V	Experimentally determined S:(A+V)	Experimentally determined composition[a]
TiV_2S_4	1273	9	0.5	0.48(2)	1.30(2)	$Ti_{0.97}V_{2.03}S_{3.90}$
CrV_2S_4	1023	7	0.5	0.51(2)	1.32(1)	$Cr_{1.01}V_{1.99}S_{3.96}$
FeV_2S_4	1023	10	0.5	0.49(2)	1.32(1)	$Fe_{0.99}V_{2.01}S_{3.96}$
NiV_2S_4	1273	6	0.5	0.50(1)	1.33(1)	$Ni_{1.00}V_{2.00}S_{3.99}$

[a]Normalised to a total metal content of three.

the neutron data for TiV_2S_4 in the region 2.2–2.5 Å. It was suggested that an additional feature observed in neutron diffraction data during an earlier study[8] of FeV_2S_4 arises from long range ordering of the two types of cation in a layer, which is not detectable by powder X-ray diffraction. The additional peaks in the data for TiV_2S_4 could not be indexed on the basis of either a primitive or a doubled unit cell and, in the absence of further evidence, it must be concluded that they arise from oxide impurity phases which have been observed previously in neutron profiles of members of the non-stoichiometric series $Ti_xV_{3-x}S_4$.[16] As these features are of such low intensity and well separated from reflections arising from the ternary sulfide, it was not felt necessary to exclude this region from the structural refinement of TiV_2S_4.

Following initial refinement of scale factors, background terms, X-ray zero-point, positional and lattice parameters, it was apparent that the agreement between observed and calculated intensities in certain regions of the neutron profiles was poor. Site occupancy factors of the cations were introduced as variables into the refinement with the constraint that the analytically determined stoichiometry was maintained. This resulted in a reduction in the weighted residuals. Owing to the presence of a measurable amount of oxide impurity in the chromium sample, the constraint on cation site occupancies was relaxed leading to a slight lowering of the occupancy of the site in the vacancy layer. No such change was observed when this constraint was removed from the refinements for the remaining materials. Refinement of site occupancy factors of the sulfide ions did not result in any significant deviation from unity and they were subsequently fixed at this value. Following introduction of thermal and peak shape parameters, the final cycle of refinement resulted in the observed, calculated and difference profiles of Fig. 2. The corresponding refined parameters are given in Table 2 and important distances and angles are presented in Tables 3 and 4.

Magnetic susceptibility data exhibit a relatively weak temperature dependence (Fig. 3). TiV_2S_4 and NiV_2S_4 appear to be paramagnetic. However, a slight anomaly in $\chi(T)$ of the latter in the region of 185 K, leading to a plot similar in form to those observed in $Ni_xCr_{3-x}S_4$ phases,[3] may indicate a transition to a long-range ordered state. For the chromium analogue, zfc and fc magnetic susceptibilities overlie each other completely at all temperatures down to the maximum in susceptibility at 15 K. Below this temperature, the two curves diverge. This behaviour indicates a magnetically frustrated system and suggests that CrV_2S_4 should be described as a spin-glass as has been proposed for other members of the $V_xCr_{3-x}S_4$ series.[19] The magnetic susceptibility of FeV_2S_4 passes through a maximum at 135(3) K. The absence of any divergence between zfc and fc data at this temperature indicates that it corresponds to a transition to a long-range ordered magnetic state rather than a spin-glass transition. After passing through a minimum at *ca.* 50 K, both susceptibilities increase on further cooling suggesting some spontaneous magnetization in the long-range ordered state. High temperature magnetic susceptibility data were not adequately described by a Curie–Weiss expression owing to curvature in the plots of reciprocal susceptibility. Therefore a modified Curie–Weiss law of the form $\chi=\chi_0+C/(T-\theta)$, incorporating a temperature independent paramagnetic term, χ_0, was fitted to the zero-field-cooled data. The derived magnetic parameters presented in Table 5 were relatively insensitive to the range of data in the paramagnetic region used in the fitting procedure.

All materials exhibit a low electrical resistivity at room temperature [Fig. 4(a)]. Although some caution is required in interpreting resistivity data obtained from sintered pellets, owing to contributions from grain boundaries, the resistivity of CrV_2S_4 clearly shows a different temperature dependence to that of the other materials and is consistent with semiconducting behaviour. Whilst attempts to fit a simple Arrhenius expression to these data were unsuccessful, a plot of $\ln(\rho)$ *vs.* $T^{-1/4}$ is linear over the temperature range $80 \leqslant T/\mathrm{K} \leqslant 270$ [Fig. 4(b)], characteristic of a variable-range-hopping conduction mechanism.[20,21] The resistivity of the other materials shows little temperature dependence, that of TiV_2S_4 and NiV_2S_4 decreasing slightly with decreasing temperature as expected for metallic materials. Close examination of the data reveals that although the resistivity of FeV_2S_4 initially decreases on cooling, below *ca.* 200 K it increases slightly. It is unlikely that this signifies a transition to an activated conduction mechanism but may indicate the dominance of grain boundary resistances at low temperatures.

Discussion

The slight contraction in lattice parameters across the series of samples leads to a decrease in unit cell volume of *ca.* 6% on moving from TiV_2S_4 to NiV_2S_4. In addition to two neighbours at *ca.* 3.3 Å resulting from lattice translation along the *b*-axis, each cation in the fully occupied layer has two cation neighbours at a comparatively short distance of *ca.* 3 Å and two at a considerably greater separation, 3.8–3.9 Å. In all cases, the ratio between the longer and shorter distance exceeds the value of 1.1 observed in ternary chromium sulfides. This ratio increases from the titanium to the iron containing material before decreasing slightly in the nickel analogue. Mean cation–anion separations are similar to those determined in related systems and decrease slightly across the series, consistent with the effects of orbital contraction. Cations lie at the centre of distorted octahedra whose bond angles lie in the range 81–104°. As in the $Ni_xCr_{3-x}S_4$ series,[3] octahedra in the fully occupied layer show the greater distortion from ideal geometry.

The main objective of this work was the investigation of the influence on the cation distribution in ternary Cr_3S_4 phases of changing the divalent ion within a metal sulfide matrix which remains effectively constant. Previous investigations have led us to suggest that the preference of a given cation for one of the two octahedral sites is affected by the relative abilities of the cations present to delocalise electron density by direct (t_{2g}–t_{2g}) overlap of cation based orbitals. Direct overlap requires the cation-cation distance to be below some critical value, R_c.[22] As a result of orbital contraction, R_c decreases as the transition series is traversed from left to right with the result that for a given cation–cation separation, those cations drawn from the earlier part of the transition exhibit the stronger t_{2g}–t_{2g} interactions. Furthermore, the six neighbours of a cation in the fully occupied layer provide greater opportunity for electron delocalisation than the two neighbours of a cation in the vacancy layer. This would suggest that early transition series cations would preferentially occupy the former sites. When the cations present are drawn from groups sufficiently far apart in the transition series, a high degree of cation partitioning may occur as in $NiCr_2S_4$.[3] However cations which are adjacent in the transition series have similar values of R_c leading to less marked site preferences in materials containing cations drawn from neighbouring groups. For example, this causes the sulfide, VCr_2S_4[2] and analogous selenide VCr_2Se_4[7] to adopt a structure, intermediate between the normal and inverse types, which closely approaches the formulation $(V_{0.5}Cr_{0.5})[V_{0.5}Cr_{1.5}]X_4$ (X = S, Se). Cations from non-adjacent groups may exhibit some slight site preference, as in the selenides $TiCr_2Se_4$ and $CrTi_2Se_4$[9] in which chromium preferentially occupies sites in the vacancy layer. The results reported here for the AV_2S_4 series are fully consistent with these observations. In particular, there is a progressive change across the series from a near-inverse structure for the titanium-containing material to a near normal structure for the nickel analogue (Fig. 5). The crystallographically determined composition of $Cr_{0.95}V_{1.96}S_4$ for the chromium material involves

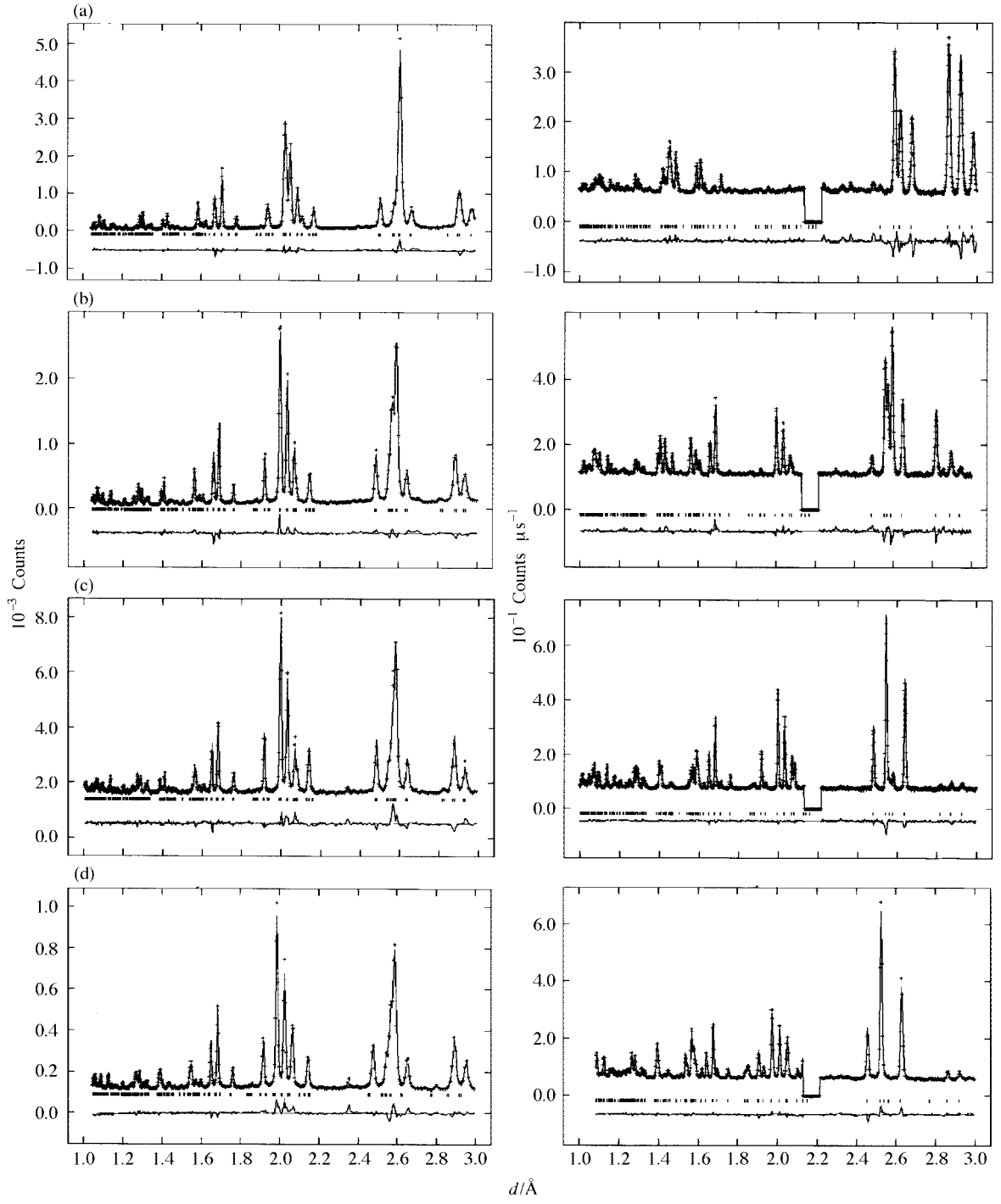

Fig. 2 Final observed (crosses), calculated (full line) and difference (lower full line) profiles for (a) TiV_2S_4, (b) CrV_2S_4, (c) FeV_2S_4 and (d) NiV_2S_4. X-Ray data appear on the left, neutron data on the right. Reflection positions are marked.

cation deficiency in the ordered vacancy layer and provides further evidence that the ordered defect structure of Cr_3S_4 is stable over a range of stoichiometry.[17] When non-stoichiometry is taken into account, the cation distribution in CrV_2S_4 corresponds to *ca.* 62% of the chromium cations occupying sites in the fully occupied layer, and the structure may be regarded as being intermediate between the normal and inverse structures, similar to that of VCr_2S_4. The iron analogue, although also adopting an intermediate structure, exhibits marked site preference effects: over 75% of the iron cations occupy sites in the vacancy layer. The cation distribution determined here is in good agreement with an earlier study,[8] using powder neutron diffraction data alone, in which refinement of the total scattering power at each site led to $(Fe_{0.72}V_{0.28})[Fe_{0.25}V_{1.75}]S_4$. This is contrary to earlier suggestions[23–25] that cation partitioning in FeV_2S_4 is complete. Partial ordering was not considered in earlier diffraction experiments and Mössbauer data appear to be a superposition of two doublets, consistent with two iron sites, rather than the symmetric doublet originally proposed. The usefulness of formal oxidation states is questionable for materials for which an ionic description appears to be less applicable than a band description. However, for the materials which adopt intermediate structures, previous work[1,9] indicates that in CrV_2S_4 the chromium substitutes in the fully occupied layer as Cr(III). It has been proposed[26] that FeV_2S_4 contains exclusively high-spin Fe(II) which was assumed to be located solely in the ordered vacancy layer. Data for $Fe_{0.1}V_{0.9}S_2$[27] in which iron is located in a MS_2 unit similar to that present in the Cr_3S_4 structure suggest that iron is present as low-spin Fe(II).

Table 2 Refined structural parameters for AV_2S_4 phases[a]

		A in AV_2S_4			
		Ti	Cr[b]	Fe	Ni
	a/Å	5.9585(5)	5.8844(1)	5.8619 (1)	5.8476(1)
	b/Å	3.3420(3)	3.3220(5)	3.29787(3)	3.28355(7)
	c/Å	11.4352(9)	11.281(2)	11.2885(1)	11.1018(3)
	β/°	91.566(2)	91.998(2)	91.995(1)	92.246(2)
	Volume/Å^3	227.63(5)	220.38(9)	218.095(3)	213.001(5)
(M)	SOF[c] A	0.145(7)	0.358(7)	0.758(2)	0.979(3)
	SOF V	0.855(7)	0.590(8)	0.242(2)	0.021(3)
	B/Å^2	0.48(7)	0.2(1)	0.66(2)	0.90(3)
[M]	SOF A	0.427(3)	0.294(5)	0.121(1)	0.011(1)
	SOF V	0.573(3)	0.683(7)	0.879(1)	0.989(1)
	x	−0.0355(3)	−0.0397(4)	−0.0526(4)	−0.040(1)
	z	0.2575(2)	0.2595(2)	0.2599(2)	0.2585(6)
	B/Å^2	0.30(4)	0.3(1)	0.17(6)	0.3(2)
S(1)	x	0.3384(3)	0.3380(5)	0.3378(2)	0.3397(4)
	z	0.3651(2)	0.3628(2)	0.3615(1)	0.3631(2)
	B/Å^2	0.28(1)	0.08(3)	0.10(1)	0.15(4)
S(2)	x	0.3344(3)	0.3370(4)	0.3372(2)	0.3367(4)
	z	0.8865(2)	0.8873(2)	0.8886(1)	0.8881(2)
	B/Å^2	0.28(1)	0.08(3)	0.10(1)	0.15(4)
R_{wp} /%	X-ray	7.1	7.8	2.9	4.6
	Neutron	2.0	2.5	1.4	2.4
	χ^2		3.2	3.9	1.4 2.3

[a]Space group: $I2/m$, (M) on 2(a) (0,0,0), [M], S(1) and S(2) on 4(i) (x,0,z). [b]Crystallographic composition: $Cr_{0.95}V_{1.96}S_4$. [c]SOF: site-occupancy factor.

Table 3 Bond distances (Å) for AV_2S_4 phases

	A in AV_2S_4			
	Ti	Cr	Fe	Ni
M(1)–S(1)	2.453(1) × 4	2.441(2) × 4	2.442(1) × 4	2.403(1) × 4
M(1)–S(2)	2.407(2) × 2	2.393(2) × 2	2.380(1) × 2	2.369(2) × 2
Mean M(1)–S	2.44	2.43	2.42	2.39
M(2)–S(1)	2.515(3)	2.474(4)	2.524(3)	2.467(7)
	2.496(2) × 2	2.487(3) × 2	2.511(2) × 2	2.453(5) × 2
M(2)–S(2)	2.393(3)	2.366(3)	2.324(3)	2.330(7)
	2.373(2) × 2	2.332(2) × 2	2.304(2) × 2	2.316(5) × 2
Mean M(2)–S	2.44	2.41	2.41	2.39
M(1)–M(2)	2.958(2)	2.944(3)	2.961(3)	2.889(7)
M(2)–M(2)	3.055(3) × 2	2.982(4) × 2	2.844(4) × 2	2.95(1) × 2
	3.799(3) × 2	3.806(5) × 2	3.926(4) × 2	3.79(1) × 2

Table 4 Selected bond angles (°) for AV_2S_4 phases

	A in AV_2S_4			
	Ti	Cr	Fe	Ni
S(1)–M(1)–S(1)	85.86(6) × 2	85.74(8) × 2	84.95(3) × 2	86.20(6) × 2
	94.14(6) × 2	94.26(8) × 2	95.06(3) × 2	93.80(6) × 2
S(1)–M(1)–S(2)	88.72(6) × 4	88.61(7) × 4	88.49(3) × 4	88.85(7) × 4
	91.28(6) × 4	91.39(7) × 4	91.51(3) × 4	91.15(7) × 4
S(1)–M(2)–S(1)	81.40(7) × 2	79.8(1) × 2	77.53(7) × 2	79.5(2) × 2
	84.07(8)	83.8(1)	82.10(9)	84.0(2)
S(1)–M(2)–S(2)	89.76(8) × 2	90.1(1) × 2	89.05(8) × 2	90.2(2) × 2
	88.06(8) × 2	88.1(1) × 2	88.12(8) × 2	84.0(2) × 2
	92.55(4) × 2	91.83(5) × 2	91.78(3) × 2	91.96(6) × 2
S(2)–M(2)–S(2)	100.29(7) × 2	101.2(1) × 2	104.16(8) × 2	101.2(2) × 2
	89.52(9)	90.9(1)	91.4(1)	90.3(3)

Similarly, Mössbauer data for structurally-related FeV_4S_8 appear to be consistent with the presence of low-spin Fe(II).[28] Therefore the possibility of the presence of both spin states in FeV_2S_4, which would contribute to the reduction of the paramagnetic moment, cannot be ruled out.

One-electron one-molecule energy level diagrams, of the type presented by Holt *et al.*[29] for ternary Cr_3S_4–type materials of the normal structure type, indicate that metallic behaviour is a consequence of overlap of t_{2g} orbitals associated with cations in the fully occupied layer. The resulting narrow $t_{2g}(\alpha)$ band is partially filled for a formal oxidation state of V(III):d^2 leading to metallic behaviour, as found for NiV_2S_4 in which $<3\%$ nickel is found in the fully occupied layer. In the near-inverse structure of TiV_2S_4, metallic behaviour is also predicted as Ti–Ti and V–V interactions are of comparable strength, and will give rise to a partially occupied t_{2g}-based band. As the A-cation is varied between these two extremes, the corresponding structural changes will influence the band structure

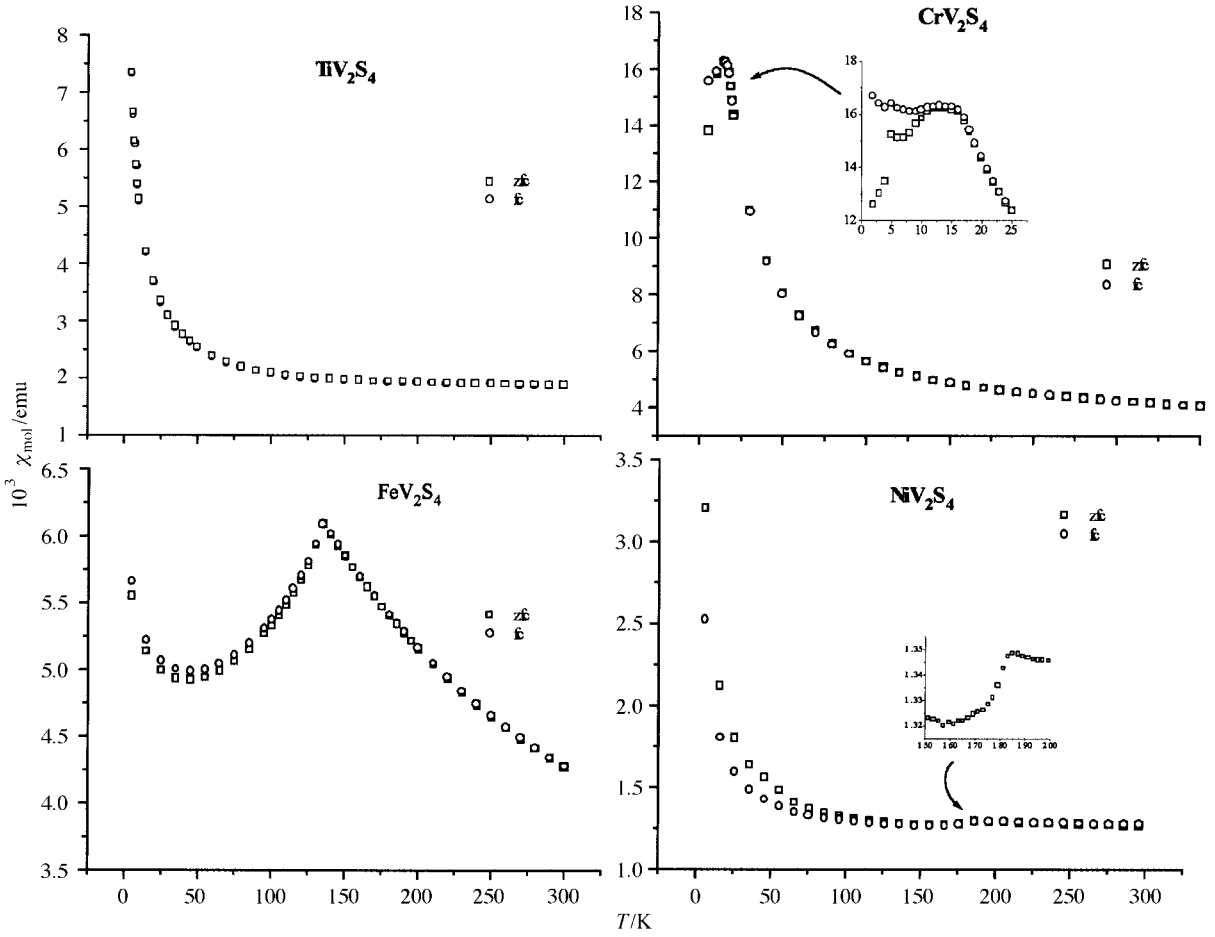

Fig. 3 Zero-field-cooled (zfc) and field-cooled (fc) molar magnetic susceptibilities for AV_2S_4 phases (A = Ti, Cr, Fe, Ni) measured in a field of 1000 G. Insets show detail around transitions.

Table 5 Parameters derived from magnetic susceptibility data for AV_2S_4

	A			
	Ti	Cr	Fe	Ni
Data range for fit (T/K)	5–300	20–300	150–300	190–286
$\chi_0/10^{-3}$ emu mol^{-1}	1.69(1)	3.22(1)	1.53(3)	1.21(1)
C/emu mol^{-1} K^{-1}	0.0442(6)	0.253(2)	1.11(2)	0.019(3)
θ/K	−2.9(1)	−2.6(1)	−108(3)	−33(18)
T_t/K	—	15(3)	135(3)	185(3)
μ_{so}(A)	2.83	4.89	4.89	2.83
μ_{exp}(A)	0.18	1.42	2.98	0.39

through changes in the Fermi energy and the band-width, together with the disorder introduced into the fully occupied layer, a full understanding of which requires detailed band structure calculations of the type performed by Dijkstra *et al.* for binary chromium chalcogenides.[30] Structural disorder due to a high degree of substitution of V(III) in the fully occupied layer by the A-cation results in a randomly fluctuating potential which can lead to the creation of localised states near the band edges.[31] When the Fermi energy lies near the boundary between localised and delocalised states, conduction is dominated by hopping of charge carriers between states localised on opposite sides of the Fermi energy. This variable-range-hopping is observed for CrV_2S_4, whereas the iron analogue exhibits metallic behaviour, suggesting that at the lower level of substitution in the fully occupied layer the Fermi level is located away from the mobility edge in a region of delocalised states.

Magnetic susceptibility investigations[32] of the isostructural binary sulfide V_3S_4 reveal that direct overlap of cation-based orbitals is sufficient to reduce the effective magnetic moment to $\leqslant 0.2\,\mu_B$. NMR studies[33] of the related ordered defect material V_5S_8 indicate the presence of two types of vanadium cations. Electrons associated with those in the fully occupied layer are itinerant and contribute to a temperature independent term in the susceptibility, whereas those associated with cations in the vacancy layer contribute to a temperature dependent term, albeit with a small effective magnetic moment. Magnetic susceptibility measurements[34] for vanadium sulfides, of a range of compositions close to the V_5S_8 stoichiometry, also indicate that only cations in the vacancy layer contribute to the effective magnetic moment and yield a moment of 2.1–2.3 μ_B per vacancy layer cation. This result is consistent with the data of De Vries and Haas[33] when the assumption is made that a single vanadium site contributes to the moment and compositional changes are taken into account. The observation of a significant temperature independent contribution to the magnetic susceptibility for all AV_2S_4 samples is in agreement with these conclusions and suggests a considerable degree of elec-

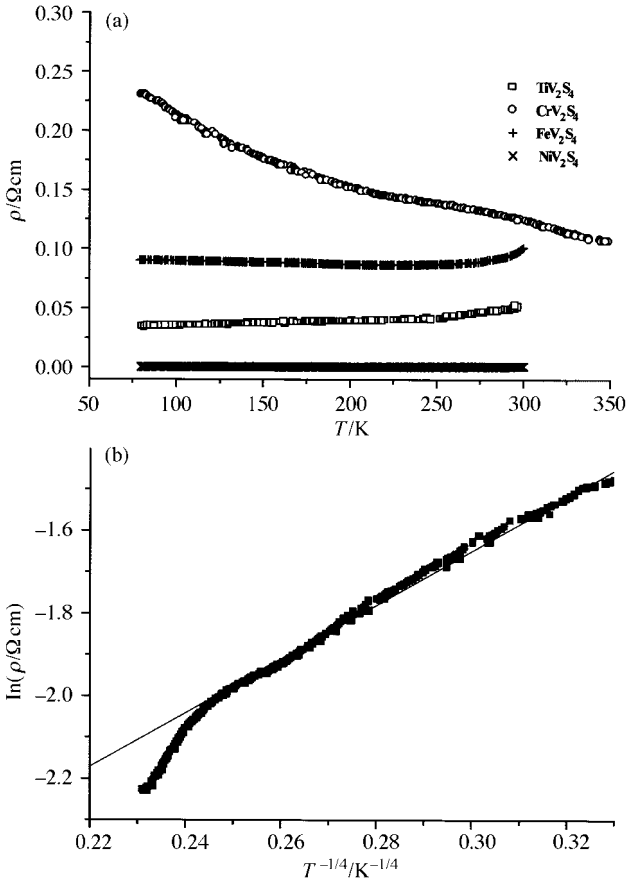

Fig. 4 Electrical data for AV_2S_4 (A = Ti, Cr, Fe, Ni): (a) resistivity as a function of temperature; (b) $T^{-1/4}$ dependence of ln(ρ) for CrV_2S_4.

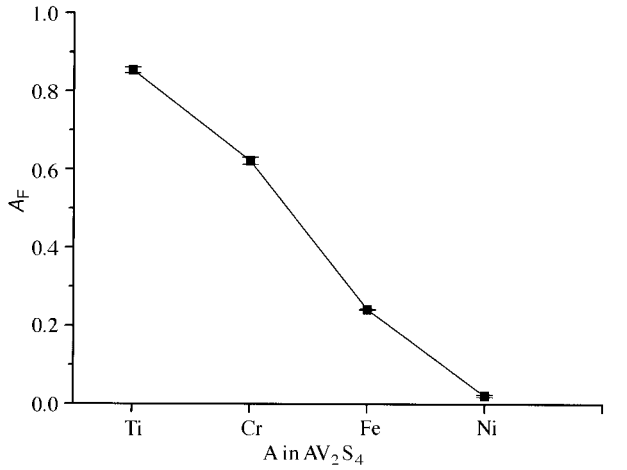

Fig. 5 The change in the fraction, A_F, of the cation A in AV_2S_4 residing in the fully occupied layer as A is varied from Ti to Ni. An occupancy of 1.0 corresponds to the inverse structure and that of 0.0, the normal structure.

tron delocalisation, consistent with the observed electron-transport properties. Application of a Curie–Weiss law to magnetic data for materials AV_2S_4 (A = Fe, Co, Ni) leads to Curie constants whose magnitudes are consistent with the absence of a moment on the vanadium ions and with spin-only behaviour of the A ion in a divalent state.[13,35] The Curie constants reported here are considerably lower than would be expected for spin-only behaviour of A(II). The source of this discrepancy appears to lie in the choice of function used to describe the data. Allowance for an appreciable temperature independent paramagnetic contribution to the susceptibility, which improves the linearity of reciprocal susceptibility plots at high temperatures, causes a marked reduction in the Curie constants as has been previously observed for the $Fe_xV_{3-x}S_4$ ($0 \leqslant x \leqslant 2$) system.[24] Removal of this temperature independent term from the fitting procedure results in Curie constants which approach more closely the values expected for spin-only behaviour of A^{2+}. Similarly low Curie constants have been observed previously during investigations of series of metallic Cr_3S_4–type phases. In the series $Ti_xV_{3-x}S_4$ ($0 \leqslant x \leqslant 3$) Tazuke *et al.*[14] observed an almost constant temperature independent susceptibility over the range $0 \leqslant x \leqslant 2$ and Curie constants which although increasing with increasing x were considerably below the values expected for localised moments, reaching a maximum of 0.1 at $x = 2$.

Spin-glass behaviour has been observed in semiconducting members of the $V_xCr_{3-x}S_4$ series in the composition range corresponding to that in which an intermediate structure is adopted, $0.4 \leqslant x \leqslant 1.0$.[1] Magnetic frustration appears to result from competing inter-layer interactions between V(II) ions in the vacancy layer and next-nearest neighbours in the fully occupied layer. Consequently, over the composition range $0.4 \leqslant x \leqslant 1.0$, the glass transition temperature decreases linearly with increasing vanadium content, reaching 32 K at $x = 1.0$. The data for CrV_2S_4 demonstrate that this reduction continues at higher vanadium contents. By contrast, magnetic data for FeV_2S_4, which are in good agreement with data presented by other workers,[24,28,35] suggest a transition to a long-range ordered state occurs below 135 K. This may be ascribed to weaker inter-layer interactions, resulting in the removal of frustration similar to the behaviour observed in $NiCr_2S_4$.[4] Preliminary powder neutron diffraction data for FeV_2S_4, collected at 4.2 K on Polaris, confirm the presence of long-range magnetic order. Additional magnetic reflections present in data from the low-resolution forward-scattering bank of detectors suggest that the magnetic structure involves a doubling of the unit cell in the a and c directions, similar to that observed in related Cr_3S_4 type phases.[4,36] However, the very poor agreement between observed and calculated data obtained by Rietveld refinement, when using data for $NiCr_2S_4$ for the initial model of the magnetic structure, suggests that the details of the magnetic structure of FeV_2S_4 differ. The combination of paucity of data and low resolution did not permit the determination of this structure and additional low-temperature high-resolution neutron data are clearly required.

Acknowledgements

We wish to thank the EPSRC for a research grant in support of our neutron scattering programme, Heriot-Watt University for a studentship for D. C. C. and The Leverhulme Trust for a research fellowship for P. V. The assistance of Dr R. I. Smith, Rutherford Appleton Laboratory, with the collection of neutron diffraction data is gratefully acknowledged.

References

1 A. V. Powell and S. Oestreich, *J. Mater. Chem.*, 1996, **6**, 807.
2 D. C. Colgan and A. V. Powell, *J. Mater. Chem.*, 1996, **6**, 1579.
3 D. C. Colgan and A. V. Powell, *J. Mater. Chem.*, 1997, **7**, 2433.
4 A. V. Powell, D. C. Colgan and C. Ritter, *J. Solid State Chem.*, 1997, **134**, 110.
5 F. Jellinek, *Acta. Crystallogr.*, 1957, **10**, 620.
6 A. Wold and K. Dwight, *Solid State Chemistry: Synthesis, Structure and Properties of Selected Oxides and Sulfides*, Chapman and Hall, New York, 1993, ch. 11.
7 A. Hayashi, Y. Ueda, K. Kosuge, H. Murata, H. Asano, N. Watanabe and F. Izumi, *J. Solid State Chem.*, 1987, **71**, 237.
8 J. M. Newsam and Y. Endoh, *J. Phys. Chem. Solids*, 1987, **48**, 607.
9 A. Hayashi, Y. Ueda, K. Kosuge, H. Murata, H. Asano, N. Watanabe and F. Izumi, *J. Solid State Chem.*, 1987, **67**, 346.
10 H. Haeuseler and W. Cordes, *Mater. Res. Bull.*, 1992, **27**, 1057.
11 W. I. F. David, M. W. Johnson, K. J. Knowles, C. M. Moreton-Smith, G. D. Crosbie, E. P. Campbell, S. P. Graham and J. S.

Lyall, Rutherford Appleton Laboratory Report, RAL–86–102, 1986.
12 A. C. Larson and R. B. Von Dreele, *General Structure Analysis System*, Los Alamos National Laboratory Report, LAUR 86–748, 1994.
13 T. Murugesan, S. Ramesh, J. Gopalakrishnan and C. N. R. Rao, *J. Solid State Chem*., 1982, **44**, 119.
14 Y. Tazuke, K. Watanabe and T. Suzuki, *J. Phys. Soc. Jpn*., 1981, **50**, 2900.
15 Y. Tazuke, *J. Phys. Soc. Jpn*., 1981, **50**, 413.
16 A. V. Powell and D. C. Colgan, *ISIS Annual Report 1998*, RB 9219, 1998.
17 D. C. Colgan and A. V. Powell, *Mater. Sci. Forum*, 1998, **278**, 686.
18 W. R. Robinson, *Acta. Crystallogr*., 1975, **31**, 1153.
19 Y. Tazuke, *J. Phys. Soc. Jpn*., 1986, **55**, 2008.
20 N. F. Mott, *J. Non-Cryst. Solids*, 1968, **1**, 1.
21 N. F. Mott, *Metal–Insulator Transitions*, Taylor and Francis, London, 1990.
22 J. B. Goodenough, *Magnetism and the Chemical Bond*, Wiley, New York, 1963.
23 H. Nozaki, H. Wada and H. Yamamura, *Solid State Commun*., 1982, **44**, 63.
24 H. Nozaki and H. Wada, *J. Solid State Chem*., 1983, **47**, 69.
25 I. Kawada and H. Wada, *Physica B*, 1981, **105**, 223.
26 S. Muranaka and T. Takada, *J. Solid State Chem*., 1975, **14**, 291.
27 F. J. Disalvo, M. Eibschütz, C. Cros, D. W. Murphy and J. W. Waszcak, *Phys. Rev. B*, 1979, **19**, 3441.
28 Y. Oka, K. Kosuge and S. Kachi, *Mater. Res. Bull*., 1977, **12**, 1117.
29 S. L. Holt, R. J. Bouchard and A. Wold, *J. Phys. Chem. Solids*, 1966, **27**, 755.
30 J. Dijkstra, C. F. van Bruggen, C. Haas and R. A. de Groot, *J. Phys.: Condens. Matter*, 1989, **1**, 9163.
31 N. F. Mott and E. A. Davis, *Electronic Processes in Non-Crystalline Materials*, 2nd edn., Oxford Univ. Press, 1979.
32 Y. Tazuke, T. Sato and Y. Miyako, *J. Phys. Soc. Jpn*., 1982, **51**, 2131.
33 A. B. De Vries and C. Haas, *J. Phys. Chem. Solids*, 1973, **34**, 651.
34 H. Nozaki, M. Umehara, Y. Ishizawa, M. Saeki, T. Mizoguchi and M. Nakahira, *J. Phys. Chem. Solids*, 1978, **39**, 851.
35 B. L. Morris, R. H. Plovnick and A. Wold, *Solid State Commun*., 1969, **7**, 291.
36 E. F. Bertaut, G. Roult, R. Aleonard, R. Pauthenet, M. Chevreton and R. Jansen, *J. Phys. (Paris)*, 1964, **25**, 582.

Paper 8/06469E